INSTITUTE OF PHYSICS PUBLISHING JOURNAL OF PHYSICS: CONDENSED MATTER

J. Phys.: Condens. Matter **14** (2002) 12099–12117 PII: S0953-8984(02)38497-2

Model colloid–polymer mixtures in porous matrices: density functional versus integral equations

Matthias Schmidt[1], **Elisabeth Schöll-Paschinger**[2], **Jürgen Köfinger**[2] **and Gerhard Kahl**[2]

[1] Institut für Theoretische Physik II, Heinrich-Heine-Universität Düsseldorf, Universitätsstraße 1, D-40225 Düsseldorf, Germany
[2] Center for Computational Materials Science and Institut für Theoretische Physik, TU Wien, Wiedner Hauptstraße 8-10, A-1040 Wien, Austria

Received 21 June 2002, in final form 22 August 2002
Published 8 November 2002
Online at stacks.iop.org/JPhysCM/14/12099

Abstract

We test the accuracy of a recently proposed density functional (DF) for a fluid in contact with a porous matrix. The DF was constructed in the spirit of Rosenfeld's fundamental measure concept and was derived for general mixtures of hard core and ideal particles. The required double average over fluid and matrix configurations is performed explicitly. As an application we consider a model mixture where colloids and matrix particles are represented by hard spheres and polymers by ideal spheres. Integrating over the degrees of freedom of the polymers leads to a binary colloid–matrix system with effective Asakura–Oosawa pair potentials, which we treat with an integral-equation theory. We find that partial pair correlation functions from both theories are in good agreement with our computer simulation results, and that the theoretical results for the demixing binodals compare well, provided the polymer-to-colloid size ratio, and hence the effect of many-body interactions neglected in the effective model, is not too large. Consistently, we find that hard (ideal) matrix–polymer interactions induce capillary condensation (evaporation) of the colloidal liquid phase.

1. Introduction

Considerable effort has been dedicated during the past years to developing theoretical tools that allow the determination of the structural and thermodynamic properties of a (continuum) fluid that is in contact with a porous matrix. Such situations are studied using 'partly quenched' or 'quenched–annealed' (QA) systems. Motivation for these activities can be traced back both to academic as well as to more practical reasons (for an overview see [1]).

(i) In experimental and theoretical studies it was found that already a minute volume fraction of matrix material can modify the phase behaviour of the fluid substantially; current investigations are dedicated to gaining a deeper insight into this phenomenon.

(ii) Fluids in contact with a porous matrix are of technological interest, with application in catalysis, gas separation and purification.

From the theoretical point of view one frequently models porous materials by frozen configurations of model fluids. The main problem in the description of such systems lies in the double average required for the calculation of thermodynamic and structural properties: one average is taken over the configurations of the liquid, keeping the matrix particles in fixed positions; the second average is then taken over different matrix configurations. This problem was solved successfully for microscopic approaches that are based on integral-equation and thermodynamic perturbation theories: introducing the replica trick (developed originally for the theory of spin glasses [2]), Given and Stell proposed a method which indeed could cope with this problem [3–5]. This approach has become meanwhile a powerful tool on which many of the present day microscopic approaches in the field are based. The replica trick exploits a mathematical isomorphism between a partly quenched system and a limiting case of a corresponding equilibrium ('replicated') system which consists of the now mobile matrix particles and of s non-interacting identical copies of the liquid. The properties of the quenched system are obtained by considering the limit $s \to 0$ of the properties of the equilibrium system, which, in turn, can be treated by standard liquid state theories. In the replica method, the so-called replica Ornstein–Zernike (ROZ) equations are introduced as the counterpart of the Ornstein–Zernike equations in standard liquid state theory, relating the liquid–liquid, the liquid–matrix and the matrix–matrix correlation functions. Thermodynamic relations for such systems that can be used to determine phase diagrams have been presented by Rosinberg, Stell and co-workers [7, 8].

Another approach that has not been treated yet is to tackle the problem with classical density functional theory (DFT). In particular during the past two or three decades, DFT has become a very powerful and attractive tool to study the structural and thermodynamic properties both of homogeneous and inhomogeneous fluid systems (for an overview see, for instance, [9]). The widespread use of DFT-based methods is to a considerable amount due to the fact that several concepts have been proposed for a constructive determination of a density functional (DF) for a given system. Restricting ourselves in this contribution to (partially penetrable) hard sphere (HS) particles and their mixtures, fundamental measure theory (FMT) is undoubtedly at present *the* approach of choice. The concept of FMT was originally introduced by Rosenfeld [10] and was alternatively formulated [11] and refined [12, 13] in subsequent work; its central idea is that the functional is derived from the geometric measures of the components of the mixture (denoted by the index i), i.e. the volume V_i, the surface S_i and the radius R_i. One of the main improvements with respect to the original idea was to include self-consistency of the functional with respect to the zero-dimensional limit which was lacking in the original FMT-DFT [10]. Nowadays, this consistency is often imposed right from the beginning by starting with the concept of the zero-dimensional limit, where the excess free energy can be calculated exactly. Then, well defined prescriptions allow the generalization to three dimensions. Successful applications of this approach include penetrable spheres that interact with a repulsive step function [14], the Asakura–Oosawa (AO) model [15] discussed below [16], the Widom–Rowlinson mixture, where particles of like species are non-interacting, while particles of unlike species experience HS repulsion [17], and also parallel [18] and rotating [19] non-spherical particles.

Recently, one of us [20] has provided a formalism of how to construct an FMT-based DF for a QA mixture of particles with ideal (vanishing) and HS interactions. Taking properly into account the double average (see above) that is required in the presence of an (ideal or HS) matrix this concept is able to provide functionals for a fluid in contact with a porous matrix.

It was found that the form of the functional is consistent with the special limiting case taken in the replica framework: the functional found for the fluid in contact with a matrix turns out to be the same as that obtained in the $s \to 0$ limit of the replicated system.

Up to now, only the formalism was presented in [20] and applied to HS mixtures; comparisons with other theories have not been performed yet. This will be done in the present contribution by comparing to results from integral-equation theory. The system we study is a model colloid–polymer mixture in contact with a porous matrix. As in the AO model the colloid particles are described by HS and globular non-adsorbing polymer coils as ideal effective spheres with a hard core cross interaction of range $R_c + R_p$, where R_c and R_p are the radii of the colloids and polymers, respectively. The AO model has been studied extensively in bulk [21–24] and recently also at walls by Brader *et al* [25]. However, confinement induced by complex pore geometries has not been considered yet and is the aim of the present work. We bring the binary AO mixture in contact with a porous matrix that is also represented by HS. Two different cases of polymer–matrix interaction are considered: first we assume HS repulsion between matrix and both colloids and polymers, hence we call this the *cp*-repelling matrix, or for short *cp*-matrix. Introducing the *cp*-matrix is a straightforward extension of the AO model, with *two* HS species where one of them is quenched and constitutes the matrix and the other is annealed and constitutes the mobile colloid component. In the second case, we envisage that due to their flexibility polymers may penetrate a porous medium easier than solid colloidal particles are able to. Hence, within our framework of effective polymer spheres, the matrix–polymer interaction should be weaker than the matrix–colloid interaction. As an extreme case, we assume ideal (vanishing) matrix–polymer interaction. The matrix only repels colloids, hence we use the term *c*-repelling matrix, or for short *c*-matrix. In both cases we deal with a ternary system which we construct following the description given earlier [20].

Starting from a description of the colloid–polymer mixture [15], by integrating out the degrees of freedom of the polymer particles [23], the fully equilibrated system can be mapped onto a one-component fluid of colloids, interacting (under certain conditions) via effective pair potentials, known in the literature as AO potentials [15]. The fluid that is in contact with a matrix becomes a two-component system with effective pair potentials: in both matrices studied here the effective interaction between colloidal particles is an AO potential; in the first case (*cp*-matrix) the colloid and matrix particles interact via an effective AO potential, while in the second case (*c*-matrix) the colloid–matrix interaction is a HS potential. For these binary systems with corresponding effective interactions we have solved the ROZ equations along with the optimized random phase approximation (ORPA) [27] as closure relation.

We have compared data for the structure functions and the phase diagram obtained from DFT and from ORPA. We find that both theories give good account of the pair correlation functions, when compared to data from our computer simulations. For moderate polymer-to-colloid size ratio $q = R_p/R_c$, where the ternary mixture can be reasonably well approximated by an effective binary model, we find that fluid–fluid demixing binodals from both theories are in good agreement. The two types of matrix considered have a qualitatively different effect on the phase behaviour. The *cp*-matrix induces capillary condensation, while the *c*-matrix leads to capillary evaporation.

The paper is organized as follows: in section 2 we introduce our model colloid–polymer–matrix mixture. The DF is constructed in section 3, where we also briefly outline the ROZ-based integral-equation approach. In section 4 we present data starting with a comparison of pair distribution functions obtained via DFT, integral-equation theory and computer simulations. We then present comparisons of phase diagrams obtained via DFT and integral-equation theory and study in particular the effects generated by varying the size ratio q. The paper is closed with a discussion and concluding remarks in section 5.

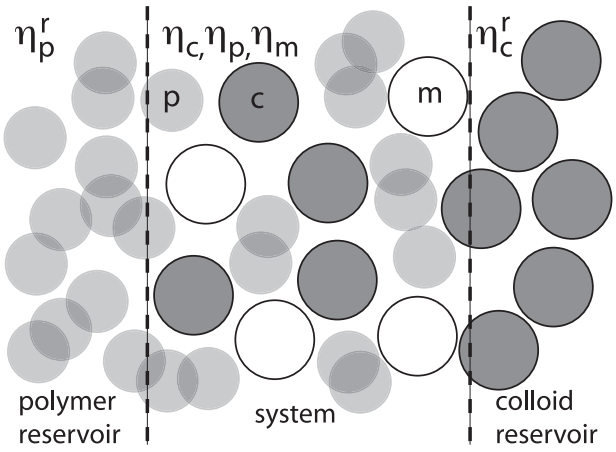

Figure 1. Illustration of the mixture of colloids (dark grey) and polymers (light grey) adsorbed in a HS matrix (white). The system (middle) is coupled to both a reservoir of polymers with packing fraction η_p^r (left), and a reservoir of colloids with packing fraction η_c^r (right). The dashed lines represent semi-permeable walls that can be penetrated solely by the corresponding reservoir species.

2. The model

In our model of a colloid–polymer mixture in contact with a porous matrix we use the following notation: the particles are characterized by radii R_i, where $i = m, c, p$ for matrix, colloid and polymer particles, and we also use the diameters $\sigma_i = 2R_i$. The interactions between the three different species are given via pair potentials $V_{ij}(r)$. In the DFT approach we will consider the full ternary system, while in the integral-equation approach we shall treat binary systems (matrix and colloid particles) with effective pair interactions $V_{ij}^{\rm eff}(r)$ obtained via integrating out the polymer degrees of freedom and truncating at the two-body level [23]. As bulk thermodynamic parameters we use the packing fractions $\eta_i = 4\pi\sigma_i^3\rho_i/3$, where ρ_i is the number density of species i. We imagine the system being in chemical equilibrium with a reservoir of pure polymers of packing fraction η_p^r, and a reservoir of pure colloids of packing fraction η_c^r, see figure 1 for an illustration. Control parameters are the two size ratios $q = R_p/R_c$ and R_m/R_c.

We shall consider three cases.

(i) In the equilibrated colloid–polymer mixture, the matrix is absent and the three pair potentials that specify the AO model are given by

$$V_{cc}(r) = \begin{cases} \infty & r \leqslant \sigma_c \\ 0 & \text{otherwise,} \end{cases} \tag{1}$$

$$V_{pp}(r) = 0, \tag{2}$$

$$V_{cp}(r) = \begin{cases} \infty & r \leqslant R_c + R_p \\ 0 & \text{otherwise.} \end{cases} \tag{3}$$

Integrating over the degrees of freedom of the polymer particles in the partition function leads to an effective interparticle potential, $V_{cc}^{\rm eff}(r)$, between the colloid particles, that features an attractive depletion attraction, $V_{\rm AO}(r)$, known in the literature as the AO potential [15]. The effective interaction in the resulting one-component system of colloids is found to be

$$\beta V_{cc}^{\rm eff}(r) = \beta V_{cc}(r) + \beta V_{\rm AO}(r)$$
$$= \begin{cases} \infty & r \leqslant \sigma_c \\ -\eta_p^r \dfrac{(1+q)^3}{q^3}\left[1 - \dfrac{3r}{2(1+q)\sigma_c} + \dfrac{r^3}{2(1+q)^3\sigma_c^3}\right] & \sigma_c < r < \sigma_c + \sigma_p \\ 0 & \sigma_c + \sigma_p < r, \end{cases} \tag{4}$$

where $\beta = 1/k_B T$, k_B is Boltzmann's constant and T is absolute temperature. It should be pointed out that this mapping is only exact for size ratios $q < 2/\sqrt{3} - 1 \approx 0.1547$. For larger q-values many-body effective potentials are non-vanishing, and using solely the pairwise contribution, equation (4), is an approximation.

(ii) The colloid–polymer mixture is in contact with an HS matrix that repels both colloids and polymers (cp-matrix). The matrix–matrix interaction is that of HS:

$$V_{mm}(r) = \begin{cases} \infty & r \leqslant \sigma_m \\ 0 & \text{otherwise.} \end{cases} \tag{5}$$

The interactions between c and p are given in (1)–(3), while the interaction between matrix and both adsorbate components is

$$V_{cm}(r) = \begin{cases} \infty & r \leqslant R_c + R_m \\ 0 & \text{otherwise,} \end{cases} \tag{6}$$

$$V_{pm}(r) = \begin{cases} \infty & r \leqslant R_p + R_m \\ 0 & \text{otherwise.} \end{cases} \tag{7}$$

The situation is depicted in the upper panel in figure 2(a). Integration over the degrees of freedom of the polymer particles leads to a binary system (lower panel in figure 2(a)); the effective interactions between colloidal particles and between colloid and matrix particles are $V_{cm}^{\rm eff}(r) = V_{cc}^{\rm eff}(r)$ as given in (4) where we have restricted ourselves to $R_c = R_m$ for simplicity.

(iii) Finally, we consider the colloid–polymer mixture in contact with a colloid-repelling matrix (c-matrix), see figure 2(b). The HS potential between matrix particles is again given via (5), while the interaction between the polymer and the matrix particles is ideal

$$V_{pm}(r) = 0. \tag{8}$$

As the polymers do not interact with the matrix no depletion attraction is generated in the binary cm-mixture and hence $V_{cm}^{\rm eff}(r) = V_{cm}(r)$ as given in (6). The effective potential between colloid particles remains an AO interaction, $V_{cc}^{\rm eff}(r)$ given in (4).

3. Theory

3.1. Free energy in the zero-dimensional limit

We first consider an idealized situation, where all particles are forced to sit on top of each other. This zero-dimensional limit can be envisaged as extreme confinement of the system inside a small cavity of particle size. The advantage is that it allows us an exact solution of the many-body problem, as the configurational integral (over all particle coordinates) becomes trivial. What remains to be considered is the statistical problem of counting the allowed particle configurations of the model under consideration. Although the detailed shape of the cavity is irrelevant, for clarity we explicitly choose a spherical pore, such that only space points

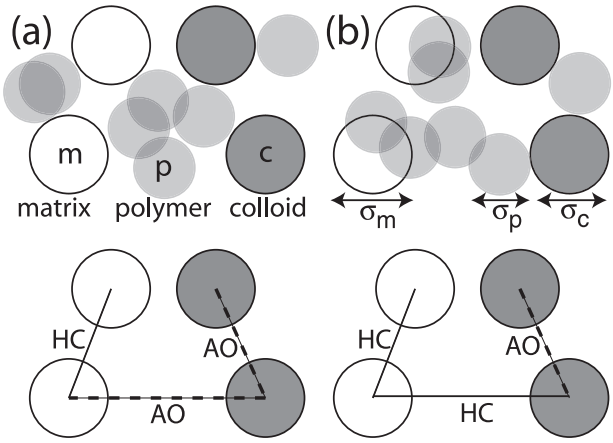

Figure 2. Sketch of the AO model of colloids (dark grey) and polymers (light grey) adsorbed in different HS matrices (white). The upper panels show the ternary mixtures with explicit polymers; the lower panels show the binary mixtures where colloid–colloid effective interactions are given by the AO potential (dashed line). The matrix particles behave as HS (solid line) without depletion attraction because they are quenched before having been brought into contact with polymers. (a) *cp*-matrix: in the ternary system all interactions are hard core except for the ideal polymer–polymer interaction. In the binary model, this leads to an effective AO potential between colloids and matrix particles. (b) *c*-matrix: in the ternary system the interactions between polymers and matrix particles are ideal; in the binary mixture the effective matrix–colloid interaction is hard core.

$\boldsymbol{r}$ with $|\boldsymbol{r}| < \epsilon$ are accessible to the particle centres, and $\epsilon \ll R_i$. This corresponds to a hard spherical pore of (i-dependent) radius $R_i + \epsilon$. Hence each particle's centre is allowed to move inside a sphere of volume $v_{0\mathrm{d}} = 4\pi\epsilon^3/3$. In the following we review the zero-dimensional free energy of the AO model without matrix, and calculate this quantity for both ternary mixtures considered in this contribution. We use the symbol A to indicate zero-dimensional Helmholtz free energies, and F for the three-dimensional case.

3.1.1. Equilibrated AO model. For the (fully equilibrated) binary AO mixture it was shown [16] that the zero-dimensional partition sum is given by

$$\Xi = z_c + \exp(z_p), \tag{9}$$

where $z_i = v_{0\mathrm{d}}\Lambda_i^{-3}\exp(\beta\mu_i)$ is the scaled fugacity, Λ_i is the (irrelevant) thermal wavelength and μ_i is the chemical potential of species $i = c, p$. The first term on the rhs of equation (9) corresponds to the state where the cavity is occupied by one colloidal particle. All states with more than one colloid are forbidden due to the HS repulsion between colloids, and therefore carry vanishing statistical weight. Hence terms of higher than linear order in z_c are absent in equation (9). The second term on the rhs of equation (9) is simply the partition sum of an ideal gas of polymers, reflecting the absence of interactions between these particles in the AO model.

From the grand potential Ω given through $\beta\Omega = -\ln\Xi$ the mean particle numbers are obtained as $\bar{\eta}_i = -z_i\partial\beta\Omega/\partial z_i$, $i = c, p$. The Helmholtz free energy is $\beta A^{\mathrm{tot}} = \beta\Omega + \sum_{i=c,p}\bar{\eta}_i\ln(z_i)$. The excess (over ideal) part is obtained by subtracting the ideal gas contribution, $\beta A = \beta A^{\mathrm{tot}} - \sum_{i=c,p}\bar{\eta}_i[\ln(\bar{\eta}_i) - 1]$. Explicitly, this leads to the zero-dimensional excess free energy,

$$\beta A(\bar{\eta}_c, \bar{\eta}_p) = (1 - \bar{\eta}_c - \bar{\eta}_p)\ln(1 - \bar{\eta}_c) + \bar{\eta}_c, \tag{10}$$

which was used in [16] as an input to derive a three-dimensional DF for the AO model.

3.1.2. AO model in a colloid- and polymer-repelling matrix. In order to calculate the zero-dimensional excess free energy for the AO model in the presence of the *cp*-matrix, we follow the same steps as above, with the important distinction of using a double QA average instead of a single one for the fully annealed system [20]. We first consider the matrix alone. Either the cavity is empty, or it carries a single matrix particle. Summing up these states in the grand ensemble yields the matrix grand partition sum,

$$\Xi_0 = 1 + z_m, \tag{11}$$

which equals the result for (fully annealed) HS, first considered (via a different route) in [12]. The grand potential is given through $\beta\Omega_0 = -\ln \Xi_0$. The average number of matrix particles is $\bar{\eta}_m = -z_m \partial\beta\Omega_0/\partial z_m$. We Legendre transform to the Helmholtz free energy, $\beta A_0^{\rm tot}(\bar{\eta}_0) = \beta\Omega_0 + \bar{\eta}_m \ln(z_m)$. Its excess part is obtained from $\beta A_0 = \beta A_0^{\rm tot} - \bar{\eta}_m[\ln(\bar{\eta}_m) - 1]$, and is explicitly given by

$$\beta A_0(\bar{\eta}_m) = (1 - \bar{\eta}_m)\ln(1 - \bar{\eta}_m) + \bar{\eta}_m. \tag{12}$$

In order to obtain the QA zero-dimensional free energy of the AO mixture, we need to average the free energy of the adsorbate over all configurations of the matrix. If the matrix is empty, the adsorbate grand partition sum is equal to the case of the fully annealed AO model (given in equation (9)). If the cavity is non-empty, i.e. is occupied by one single matrix particle, the HS potentials between matrix and colloid and between matrix and polymers prohibit the presence of any adsorbate particles, and hence the only allowed state is free of colloids and polymers. Summarizing, the adsorbate grand partition sum is given by

$$\Xi_1 = \begin{cases} z_c + \exp(z_p) & \text{no matrix particle} \\ 1 & \text{otherwise.} \end{cases} \tag{13}$$

The adsorbate free energy is then obtained as the average over all matrix realizations of $-k_B T \ln \Xi_1$, with the appropriate statistical weight according to the matrix partition sum, equation (11); note that Ξ_1 still depends on the matrix configuration. The weight is given by $1/\Xi_0$ for the first, and by z_m/Ξ_0 for the second line in equation (13). Hence the (scaled) zero-dimensional adsorbate grand potential is

$$\beta\Omega_1 = -\frac{\ln(z_c + \exp(z_p))}{1 + z_m}. \tag{14}$$

Albeit a standard Legendre transformation, we again briefly sketch the necessary steps to obtain the corresponding Helmholtz free energy, A_1. The average particle numbers of adsorbate particles are given as $\bar{\eta}_i = -z_i \partial\beta\Omega_1/\partial z_i$, $i = c, p$, and the Helmholtz free energy is obtained as $\beta A_1^{\rm tot} = \beta\Omega_1 + \sum_{i=c,p} \bar{\eta}_i \ln(z_i)$. The excess part is found by subtracting the (adsorbate) ideal gas contribution, $\beta A_1 = \beta A_1^{\rm tot} - \sum_{i=c,p} \bar{\eta}_i[\ln(\bar{\eta}_i) - 1]$. The final result is

$$\beta A_1(\bar{\eta}_m; \bar{\eta}_c, \bar{\eta}_p) = (1 - \bar{\eta}_m - \bar{\eta}_p - \bar{\eta}_c)\ln(1 - \bar{\eta}_m - \bar{\eta}_c) + \bar{\eta}_c - (1 - \bar{\eta}_m)\ln(1 - \bar{\eta}_m). \tag{15}$$

3.1.3. AO model in a colloid-repelling matrix. In the case of the *c*-matrix, the matrix is a HS fluid that repels only colloids but is penetrable to the polymers. $A_0(\bar{\eta}_m)$ is again given by equation (12). The allowed adsorbate states are the following: if the cavity is empty, the situation is the same as above (first line on the rhs of equation (13)). If the cavity is occupied by a single colloid, however, an arbitrary number of polymers may be present, as the interaction between matrix particles and polymers is ideal. We obtain

$$\Xi_1 = \begin{cases} z_c + \exp(z_p) & \text{no matrix particle} \\ \exp(z_p) & \text{otherwise.} \end{cases} \tag{16}$$

Following the same steps as above yields the Helmholtz excess free energy for the adsorbate,

$$\beta A_1(\bar{\eta}_m;\bar{\eta}_c,\bar{\eta}_p) = (1-\bar{\eta}_m-\bar{\eta}_c)\ln(1-\bar{\eta}_m-\bar{\eta}_c) - \bar{\eta}_p\ln(1-\bar{\eta}_c) + \bar{\eta}_c - (1-\bar{\eta}_m)\ln(1-\bar{\eta}_m). \tag{17}$$

3.1.4. Relation to the replica trick. Using the replica trick one starts from a fully equilibrated system, in which the adsorbate species are replicated s times. Particles of different replicas do not interact among each other (their interactions are ideal), but interact with the matrix particles in the same fashion. For such replicated models the above formalism (section 3.1.1) may be applied, and the zero-dimensional excess free energy, A_2, of the replicated system is obtained. The zero-dimensional QA free energy is the limit $A_1 = \lim_{s\to 0}[\partial \exp(-A_2)/\partial s]\exp(A_2)$. One can show that for the models considered here $A_2 = A_0(\bar{\eta}_m) + sA_1(\bar{\eta}_m;\bar{\eta}_c,\bar{\eta}_p)$. Hence the free energy obtained from the replica trick is equal to the result from the explicit double average, $A_1 = A_2$.

3.2. Density functional theory

3.2.1. Geometry-based free energy functional. Returning to three dimensions, we apply well tried geometrical recipes to derive approximative DFTs [10, 12–14, 16, 17]. The formalism requires as input the zero-dimensional excess free energy A of the model under consideration and yields as an output (an approximation for) the three-dimensional excess free energy functional, F^{exc}. It can be applied to either the pure matrix, where $A = A_0$, to the adsorbate, $A = A_1$, or even to the replicated system, $A = A_2$. Within the framework, the excess Helmholtz free energy is expressed as

$$F^{\text{exc}}[\{\rho_i(\boldsymbol{r})\}] = k_BT\int \mathrm{d}^3x\ \Phi(\{n_\alpha^{(i)}(\boldsymbol{x})\}), \tag{18}$$

where $\{\rho_i(\boldsymbol{r})\}$ is the set of all density profiles. The reduced free energy density Φ is a function of a set of weighted densities $\{n_\alpha^{(i)}(\boldsymbol{x})\}$, where i labels the species and α the type of weighted density. The weighted densities are obtained by convolutions of the actual density profiles with weight functions $w_\alpha^{(i)}$, explicitly given as

$$n_\alpha^{(i)}(\boldsymbol{x}) = \int \mathrm{d}^3r\ \rho_i(\boldsymbol{r})w_\alpha^{(i)}(\boldsymbol{x}-\boldsymbol{r}). \tag{19}$$

As all non-vanishing interactions are HS interactions, it is sufficient to take the usual fundamental measure weight functions [10, 13], which recover (upon convolution) the Mayer bonds $\exp(-\beta V_{ij}(r)) - 1$. The weight functions are defined as

$$w_3^{(i)}(\boldsymbol{r}) = \Theta(R_i - r), \qquad w_2^{(i)}(\boldsymbol{r}) = \delta(R_i - r), \tag{20}$$

$$\boldsymbol{w}_{\text{v2}}^{(i)}(\boldsymbol{r}) = w_2^{(i)}(\boldsymbol{r})\,\boldsymbol{r}/r, \qquad \hat{\boldsymbol{w}}_{\text{t2}}^{(i)}(\boldsymbol{r}) = w_2^{(i)}(\boldsymbol{r})\left[\frac{\boldsymbol{r}\boldsymbol{r}}{r^2} - \hat{\mathbf{1}}/3\right], \tag{21}$$

where $r = |\boldsymbol{r}|$, $\Theta(r)$ is the Heaviside step function, $\delta(r)$ is the Dirac distribution, $\boldsymbol{r}\boldsymbol{r}$ is a dyadic product and $\hat{\mathbf{1}}$ is the rank-two unit tensor. Further, linearly dependent, weights are $w_1^{(i)}(\boldsymbol{r}) = w_2^{(i)}(\boldsymbol{r})/(4\pi R_i)$, $\boldsymbol{w}_{\text{v1}}^{(i)}(\boldsymbol{r}) = \boldsymbol{w}_{\text{v2}}^{(i)}(\boldsymbol{r})/(4\pi R_i)$, $w_0^{(i)}(\boldsymbol{r}) = w_1^{(i)}(\boldsymbol{r})/R_i$. The weight functions $w_\alpha^{(i)}$ have dimension of length$^{3-\alpha}$. They differ in their tensorial rank: $w_0^{(i)}, w_1^{(i)}, w_2^{(i)}, w_3^{(i)}$ are scalars; $\boldsymbol{w}_{\text{v1}}^{(i)}, \boldsymbol{w}_{\text{v2}}^{(i)}$ are vectors (subscript v); $\hat{\boldsymbol{w}}_{\text{t2}}^{(i)}$ is a rank-two tensor (subscript t). This formulation is equivalent to the tensorial formalism in [26], see equations (1.16), (1.17) therein. In principle, the rank-three tensorial form introduced in [26] could be used for problems where the dimensional crossover is delicate.

We determine the functional dependence of Φ on the weighted densities by imposing the exact crossover to zero dimensions, where $\rho_i(\boldsymbol{r}) = \bar{\eta}_i\delta(\boldsymbol{r})$, and follow recent treatments of FMT [13, 26] by considering multi-cavity limits to obtain $\Phi = \Phi_1+\Phi_2+\Phi_3$, with contributions

$$\Phi_1 = n_0^{(i)}\varphi_i(\{n_3^{(l)}\}), \tag{22}$$

$$\Phi_2 = (n_1^{(i)}n_2^{(j)} - \boldsymbol{n}_{\mathrm{v}1}^{(i)}\cdot\boldsymbol{n}_{\mathrm{v}2}^{(j)})\varphi_{ij}(\{n_3^{(l)}\}), \tag{23}$$

$$\Phi_3 = \frac{1}{8\pi}(n_2^{(i)}n_2^{(j)}n_2^{(k)}/3 - n_2^{(i)}\boldsymbol{n}_{\mathrm{v}2}^{(j)}\cdot\boldsymbol{n}_{\mathrm{v}2}^{(k)} + \tfrac{3}{2}[\boldsymbol{n}_{\mathrm{v}2}^{(i)}\hat{\boldsymbol{n}}_{\mathrm{t}2}^{(j)}\boldsymbol{n}_{\mathrm{v}2}^{(k)} - \mathrm{tr}(\hat{\boldsymbol{n}}_{\mathrm{t}2}^{(i)}\hat{\boldsymbol{n}}_{\mathrm{t}2}^{(j)}\hat{\boldsymbol{n}}_{\mathrm{t}2}^{(k)})])\varphi_{ijk}(\{n_3^{(l)}\}), \tag{24}$$

where the repeated-index summation convention is used, derivatives of the zero-dimensional excess free energy are $\varphi_{i\ldots k}(\{\bar{\eta}_l\}) \equiv \partial^m\beta A_\tau(\{\bar{\eta}_l\})/\partial\bar{\eta}_i\ldots\partial\bar{\eta}_k$ and tr denotes the trace. For $\tau = 0, 1, 2$, functionals F_τ^{exc} for matrix, adsorbate and replicated system are obtained, respectively. Two routes to the QA free energy functional are possible: either directly through A_1, giving F_1^{exc}, or via application of the replica trick to F_2^{exc}. The results from the two routes can be shown to be equal, $F_1^{\mathrm{exc}} = F_2^{\mathrm{exc}}$, which is a sign of internal consistency of the current approach.

3.2.2. Minimization principle. For reasons of completeness, we give the general strategy for how to apply the theory to an inhomogeneous problem. One first needs to obtain the matrix density profiles from minimization (with respect to the matrix density field $\rho_m(\boldsymbol{r})$) of the grand potential functional

$$\tilde{\Omega}_0[\rho_m(\boldsymbol{r})] = F_0^{\mathrm{exc}}[\rho_m(\boldsymbol{r})] + k_BT\int \mathrm{d}^3r\,\rho_m(\boldsymbol{r})[\ln(\rho_m(\boldsymbol{r})\Lambda_m^3) - 1] + \int \mathrm{d}^3r\,[V_m^{\mathrm{ext}}(\boldsymbol{r}) - \mu_m]\rho_m(\boldsymbol{r}), \tag{25}$$

where V_m^{ext} is an external potential acting on m, generating matrix inhomogeneities. (In our subsequent study, section 4, we only consider matrices that are spatially uniform on average, hence $V_m^{\mathrm{ext}}(\boldsymbol{r}) = 0$.) At the minimum

$$\frac{\delta\tilde{\Omega}_0}{\delta\rho_m(\boldsymbol{r})} = 0. \tag{26}$$

Once $\rho_m(\boldsymbol{r})$ is known, the adsorbate densities are obtained from minimization (only with respect to the adsorbate density distributions $\rho_c(\boldsymbol{r})$ and $\rho_p(\boldsymbol{r})$) of the grand potential

$$\tilde{\Omega}_1[\rho_m(\boldsymbol{r});\rho_c(\boldsymbol{r}),\rho_p(\boldsymbol{r})] = F_1^{\mathrm{exc}}[\rho_m(\boldsymbol{r});\rho_c(\boldsymbol{r}),\rho_p(\boldsymbol{r})] + k_BT\int \mathrm{d}^3r\sum_{i=c,p}\rho_i(\boldsymbol{r})[\ln(\rho_i(\boldsymbol{r})\Lambda_i^3) - 1] + \int \mathrm{d}^3r\sum_i[V_i^{\mathrm{ext}}(\boldsymbol{r}) - \mu_i]\rho_i(\boldsymbol{r}), \tag{27}$$

where V_i^{ext} act on species $i = c, p$, and $\rho_m(\boldsymbol{r})$ is treated as a *fixed input quantity*. Again, at the minimum

$$\frac{\delta\tilde{\Omega}_1}{\delta\rho_c(\boldsymbol{r})} = 0, \qquad \frac{\delta\tilde{\Omega}_1}{\delta\rho_p(\boldsymbol{r})} = 0. \tag{28}$$

3.2.3. Direct correlation functions. From the excess free energy functionals F_0^{exc} and F_1^{exc} given in section 3.2.1 one obtains direct correlation functions $c_{ij}(r)$ by calculating functional

derivatives and setting the density profiles to constant values. Explicitly for matrix and fluid species:

$$c_{mm}(r) = \left.\frac{\partial^2 \beta F_0^{\mathrm{exc}}}{\partial \rho_m(\boldsymbol{r}) \partial \rho_m(\boldsymbol{r}')}\right|_{\rho_m = \mathrm{const}}, \tag{29}$$

$$c_{ij}(r) = \left.\frac{\partial^2 \beta F_1^{\mathrm{exc}}}{\partial \rho_i(\boldsymbol{r}) \partial \rho_j(\boldsymbol{r}')}\right|_{\rho_i, \rho_j, \rho_m = \mathrm{const}}, \qquad ij \neq mm, \tag{30}$$

where $r = |\boldsymbol{r} - \boldsymbol{r}'|$. Performing these calculations yields analytical expressions for the $c_{ij}(r)$, which are similar to the bulk AO case discussed in [16]. We will use these results below in our study of the liquid structure.

3.3. Integral-equation approach

Integral-equation approaches to calculate the structural and thermodynamic behaviour of fluids in contact with a porous matrix have been derived in the framework of the replica formalism. As shown by Given and Stell [3–5] one can relate the properties of the QA mixture to those of a fully equilibrated $(s + 1)$-component mixture: the latter consists of the now mobile matrix particles and of s non-interacting identical copies of the liquid. Using standard liquid state methods [6] for the equilibrated mixture and taking appropriately the limit $s \to 0$ one obtains expressions that allow the determination of the structural and thermodynamic properties of the QA system.

The structure functions (i.e. total and direct correlation functions $h_{ij}(r)$ and $c_{ij}(r)$ between the different particle species involved) are obtained from a numerical solution of the ROZ equations, the counterpart of the Ornstein–Zernike equations of equilibrium fluids; they read

$$h_{mm}(r) = c_{mm}(r) + \rho_m[c_{mm} \otimes h_{mm}](r), \tag{31}$$

$$h_{mc}(r) = c_{mc}(r) + \rho_0[c_{mm} \otimes h_{mc}](r) + \rho_c[c_{mc} \otimes h_{cc}](r) - \rho_c[c_{mc} \otimes h_{cc'}](r), \tag{32}$$

$$h_{cc}(r) = c_{cc}(r) + \rho_0[c_{mc} \otimes h_{mc}](r) + \rho_c[c_{cc} \otimes h_{cc}](r) - \rho_c[c_{cc'} \otimes h_{cc'}](r), \tag{33}$$

$$h_{cc'}(r) = c_{cc'}(r) + \rho_m[c_{mc} \otimes h_{mc}](r) + \rho_c[c_{cc} \otimes h_{cc'}](r) + \rho_c[c_{cc'} \otimes h_{cc}](r) - 2\rho_c[c_{cc'} \otimes h_{cc'}](r), \tag{34}$$

where $\otimes$ denotes convolution, and index c' denotes a colloidal particle from a different replica. Once the correlation functions are known one can calculate the thermodynamic properties. In our case we have solved the ROZ equations along with the ORPA closure relation [27] which allows us to determine explicit expressions for the thermodynamic properties; they are summarized along with the details of the numerical solutions in [28]. Coexistence curves are obtained from solution of the phase coexistence conditions.

4. Results

4.1. Structural correlations

As a first quantitative test of the accuracy of both theoretical approaches, we investigate the partial pair correlation functions $g_{ij}(r) = 1 + h_{ij}(r)$. To provide benchmark results, we have carried out Monte Carlo (MC) computer simulations in the canonical ensemble with 1026 particles. Statistics for the $g_{ij}(r)$ were obtained by averaging over 20 independent matrix realizations obtained from equilibrium MC simulation. For each matrix realization 10^5 MC moves per particle were performed.

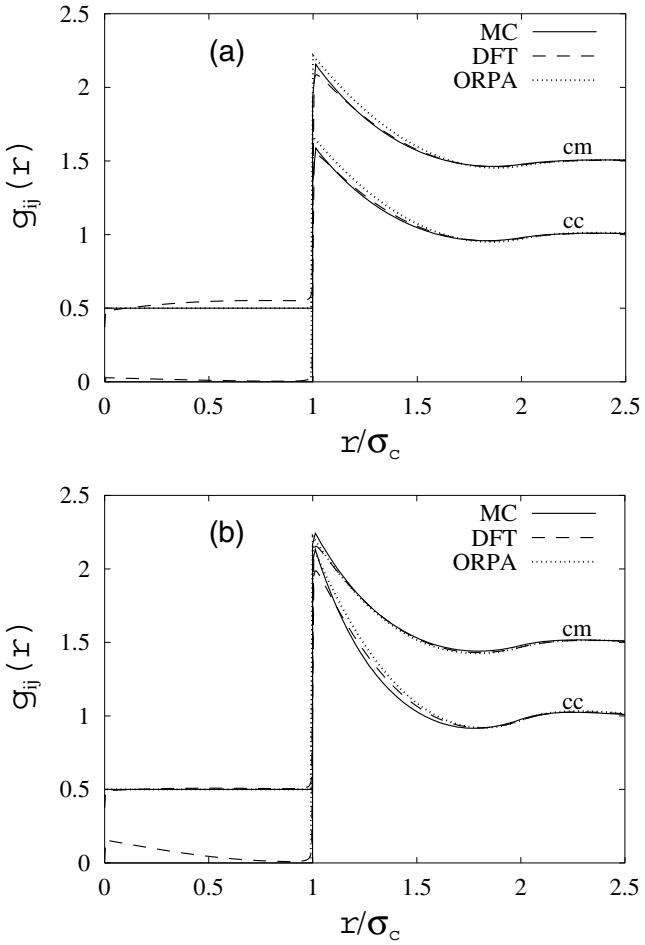

Figure 3. Partial pair correlation functions $g_{cc}(r)$ and $g_{cm}(r)$ for the AO model adsorbed in a HS matrix as a function of r/σ_c for equal sizes $\sigma_m = \sigma_c = \sigma_p$ obtained from DFT, ORPA and MC computer simulations. (a) cp-matrix for $\eta_m = \eta_c = \eta_p = 0.06$. (b) c-matrix for $\eta_m = \eta_c = \eta_p = 0.1$. The cm-curves are shifted upward by 0.5 for clarity.

In order to obtain the $g_{ij}(r)$ from DFT, we use the analytical approximations for the $c_{ij}(r)$ (see section 3.2.3) in conjunction with the ROZ equations (the generalization of equations (31)–(34) to ternary systems [29]). Within our approximate DF, direct correlation functions for particles of different replicas vanish identically, $c_{cc'} = 0$, etc. This ROZ route constitutes a severe test of the DF, as the approximation is performed on the level of $F^{\rm exc}$ and two (functional) derivatives will in general enhance any inaccuracies.

Figure 3 shows the partial pair correlations that concern no polymer species, i.e. $g_{cc}(r)$ and $g_{cm}(r)$, as functions of the scaled distance r/σ_c. We do not display the $g_{mm}(r)$ which are simply the HS pair correlation functions. For simplicity we restrict ourselves to equal sizes ($\sigma_m = \sigma_c = \sigma_p$, i.e. $q = 1$) and consider the two matrices introduced above: in figure 3(a) we show results for the cp-matrix for packing fractions $\eta_m = \eta_c = \eta_p = 0.06$. In figure 3(b) we consider the c-matrix ; due to the polymer penetrability we can choose somewhat higher packing fractions, $\eta_m = \eta_c = \eta_p = 0.1$, while still staying away safely from any (demixing)

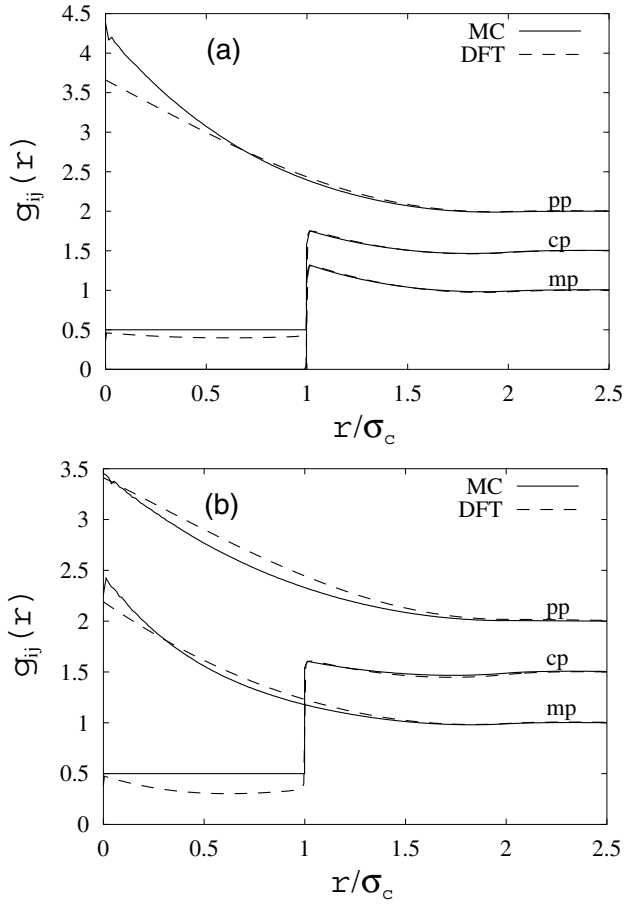

Figure 4. Partial pair correlation functions $g_{ij}(r)$ for the AO model adsorbed in an HS matrix as a function of r/σ_c for equal sizes $\sigma_m = \sigma_c = \sigma_p$ obtained from DFT and MC computer simulations. (a) *cp*-matrix for $\eta_m = \eta_c = \eta_p = 0.06$. (b) *c*-matrix for $\eta_m = \eta_c = \eta_p = 0.1$. The curves are shifted upward by 0.5 for clarity, as labelled.

phase boundary. We emphasize that the matrix packing fractions considered in this part of our study are relatively large compared to experimental studies. The densities we investigate are moderate, i.e. overall densities are $\eta_c + \eta_p + \eta_m = 0.18$ in case of the *cp*-matrix and 0.3 in case of the *c*-matrix. We believe that such densities constitute non-trivial tests of the theories. A stronger test would be provided by approaching the demixing phase boundary by increasing colloid and polymer densities, an issue that we leave for possible future work.

The general agreement of the results from DFT and ORPA with MC data is in both cases very good. The DFT result slightly violates the core conditions, $g_{cc}(r < 2R_c) = 0$ and $g_{cm}(r < R_c + R_m) = 0$. It is even closer to the MC result than the ORPA outside the core. Undoubtedly a certain amount of the differences can be attributed to the fact that the MC and DFT results are obtained for the full ternary system, while ORPA data are calculated for a binary system with effective forces, neglecting three- and higher-body forces for $q > 0.1547$. In particular for the large q-value chosen here ($q = 1$), this truncation has non-negligible effects. Summarizing we can conclude that DFT and ORPA are capable of describing the fluid correlations correctly.

The other pair correlation functions concern correlations with polymer particles, namely, $g_{mp}(r)$, $g_{cp}(r)$ and $g_{pp}(r)$. These functions can be obtained if the full ternary system is treated (as this is the case in the DFT approach); in the ORPA, where we consider only the binary system with effective pair interactions, information about these correlation functions is lost. In figure 4 the DFT results are shown and again compared to MC data. We observe pronounced differences between the results for the *cp*-matrix and the *c*-matrix in the behaviour of $g_{mp}(r)$ for $r < R_m + R_p$, demonstrating the tendency for polymers to sit on the top of the matrix particles in the case of the *c*-matrix. Again agreement between MC and DFT results is satisfactory.

4.2. Fluid demixing

We next investigate the fluid demixing phase diagram of the model colloid–polymer mixture in contact with the matrix. The parameter q plays here an important role. While for $q < 0.1547$ the above mentioned mapping of the ternary system onto a binary system with effective pair potentials is exact, we did not choose q-values that are that small, since only for $q \gtrsim 0.35$ does the fluid–fluid transition become stable with respect to the freezing transition [22, 23]. As a compromise we have therefore chosen as the lowest value $q = 0.3$, and compare how the (possibly metastable) demixing binodals from ORPA and DFT are affected by the presence of the matrix. Here and in the following we have chosen equal sizes for the matrix and the colloid particles, $\sigma_m = \sigma_c$. The matrix packing fraction is $\eta_m = 0.05$; here we know [29] that for matrix packing fractions larger than $\sim$0.1 discrepancies between computer simulation data and ORPA results are observed.

We display the binodal in two different representations (see figure 5): first, in the (η_c, η_p^r)-plane (left panels in figure 5), corresponding to the density versus inverse temperature representation for a simple fluid; second, in the (η_c^r, η_p^r)-plane (right panels in figure 5), where η_c^r is the packing fraction of colloids in a reservoir of pure colloids. η_c^r is obtained by equating the colloid chemical potential of the system and of the colloid reservoir (within the DFT the expression for the reservoir chemical potential is identical to the Percus–Yevick compressibility result). As the relation between η_c^r and the colloid chemical potential is monotonic, the second representation corresponds to a chemical potential versus inverse temperature phase diagram. Note that if we consider the binary model with effective pair interactions (as done in the ORPA treatment), we need to take into account the one-body polymer contribution that emerges in the partition sum. This generates an *additive* constant $k_B T \eta_p^r (1+q)^3/q^3$ to the colloid chemical potential, which does not affect phase equilibria, but needs to be taken into account when assuming equilibrium with a *pure* system of colloids with fraction η_c^r.

In figure 5 we show the phase diagrams obtained from DFT and ORPA for the bulk (no matrix) colloid–polymer mixture and for the case where this mixture is in contact with the *cp*-matrix or *c*-matrix. Comparing the bulk case with the computer simulation results by Bolhuis *et al* [24] for a similar size ratio ($q = 0.34$) we find that the ORPA fares better, indicating that the accuracy of the free volume free energy worsens for strongly asymmetric size ratios. (Note that ORPA results in figure 5(b) are displayed only in a smaller η_p^r-interval, as the solution of the integral equations becomes involved as we proceed to higher polymer densities.) The effect of both matrices is to shift the critical point and hence the binodal toward larger η_p^r, corresponding to the common shift of the critical point to smaller temperatures in simple fluids. In the *cp*-matrix case, we observe only a rather small effect. This is understandable as matrix and colloid particles interact in a similar way with the polymer particles (HS interactions with polymers in the ternary model, AO attraction in the binary model with effective interactions), and the critical colloid packing fraction is large compared to the η_m. Hence in this case where a small portion of identical particles is quenched the effect of the matrix is only a minor one. For

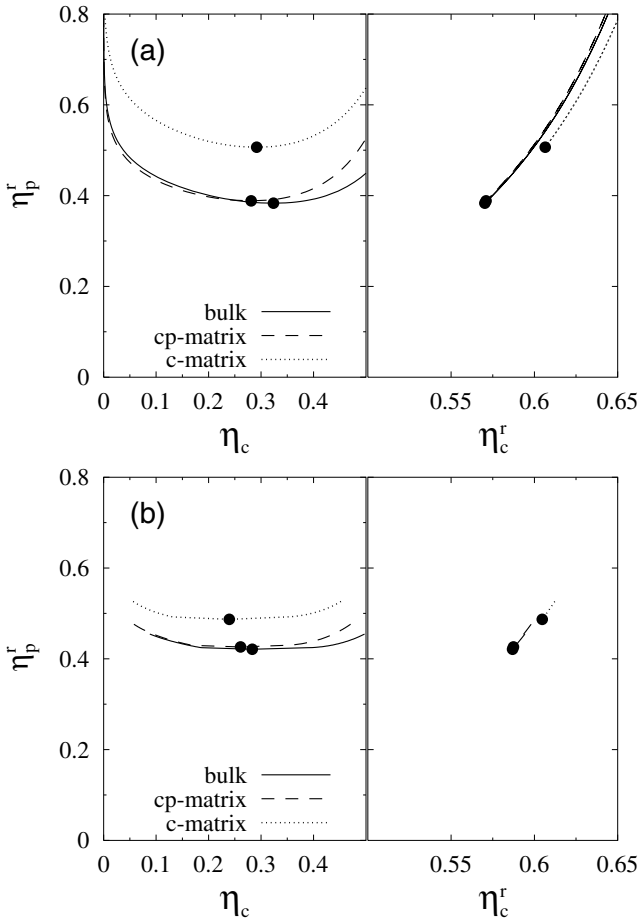

Figure 5. Demixing phase diagram for the model colloid–polymer mixture in contact with different HS matrices as a function of η_c, η_p^r (left panels) and η_c^r, η_p^r (right panels) for $\eta_m = 0.05$ and size ratios $q = 0.3$, $\sigma_m/\sigma_c = 1$. Tielines between coexisting phases are horizontal in the left panels. (a) DFT result, (b) ORPA result.

the c-matrix we observe a considerably larger effect: the presence of matrix particles that can be penetrated by polymers (and which consequently do not feature depletion attraction in the effective system) shifts the critical point and the binodal toward larger η_c^r, reflecting capillary evaporation. The ORPA results in figure 5(b) show the same tendencies for the shift of the critical point as observed in DFT, however the effects are quantitatively smaller.

Increasing the size ratio to $q = 0.6$ we expect the fluid demixing phase transition to be stable with respect to the freezing transition [23]; results for this case are depicted in figure 6. Again comparing the bulk case to the simulations for $q = 0.67$ [24] we find that both theories predict the binodal and the location of the critical point reasonably well. It is manifest that in the case of the *cp*-matrix the critical point and the binodal shift to *smaller* η_c^r, reflecting capillary condensation of the colloidal liquid phase. In contrast, we observe that the c-matrix shifts the critical point and the binodal to *larger* η_c^r which is the indication of capillary evaporation of the colloid liquid. The qualitatively different behaviour is predicted consistently in DFT and ORPA.

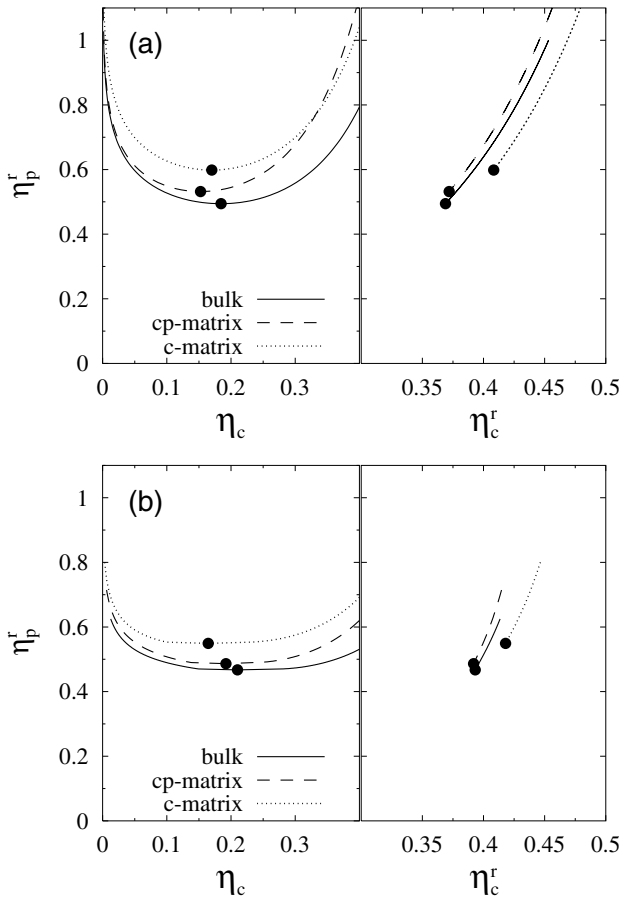

Figure 6. The same as figure 5, but for size ratio $q = 0.6$.

Finally, we display results for size ratio $q = 1$ in figure 7. This is a rather large q-value, where many-body contributions to the effective interactions of the binary system must be considered as important, hence the mapping from the ternary to the binary system with effective pair potentials is certainly questionable. Certainly as a consequence of this fact, marked differences in the binodals between both theories are observed.

(i) Within the ORPA the bulk critical point (and hence the binodal) is shifted toward larger η_c and smaller η_p^r compared to the treatment of the full mixture (DFT). A similar trend was found before in a comparison of free-volume theory and perturbation theory for the AO potential [23] (see the results for $q = 0.8$ therein). Note also that the free volume result is quite accurate for large size ratios compared to simulation results ($q = 1.05$ in [24]).

(ii) In the DFT a crossover has occurred, namely the c-matrix shifts the binodal to *higher* values of η_p^r than the cp-matrix, while this now reversed succession is not predicted by the ORPA. In addition, the binodals in the (η_c^r, η_p^r)-representation have different slopes in ORPA and DFT.

We attribute these differences rather to the above mentioned differences in the models considered, than to the respective theoretical treatments.

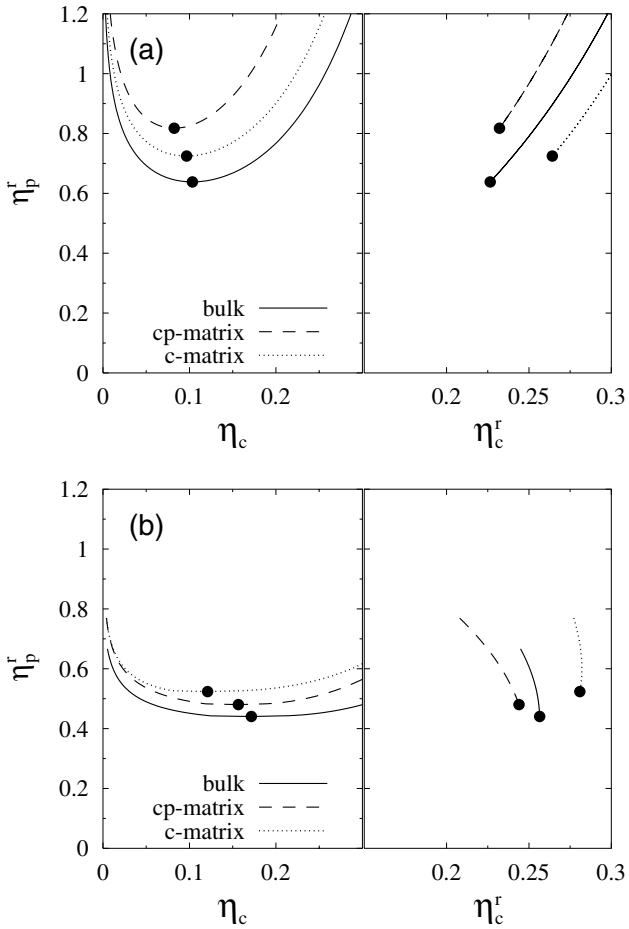

Figure 7. The same as figure 5, but for size ratio $q = 1$.

As our DFT treatment operates on the level of the full ternary system, the system polymer packing fraction, η_p, is easily accessible. In figure 8 we display the demixing binodal in the (η_c, η_p)-plane (left panel). Qualitatively different behaviour emerges for the two types of matrix: the *cp*-matrix promotes demixing, while the *c*-matrix suppresses demixing. Finally, in the (η_c^r, η_p)-representation again we observe the binodal shift toward higher η_c^r. The same trend is observed for the larger size ratios $q = 0.6$ (figure 9) and $q = 1$ (figure 10).

5. Conclusions

In this paper we have compared results for the structure and the phase behaviour of a model colloid–polymer mixture that is in contact with a porous matrix. All interparticle interactions encountered in this ternary system are either HS-like or ideal. We have first considered the pure bulk mixture (colloids—HS—and polymers—ideal particles) and have then brought this fluid into contact with a porous matrix, represented by HSs.

We have studied two cases, the *cp*-matrix where the matrix and the polymer particles interact as HSs and the *c*-matrix where the polymer particles are allowed to overlap the matrix

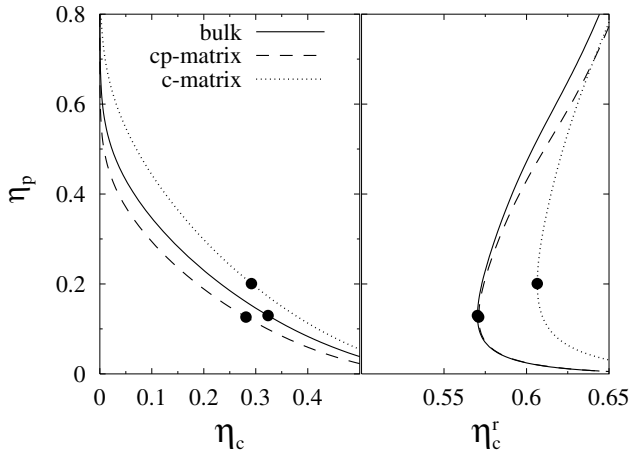

Figure 8. DFT result for the demixing phase diagram for the model colloid–polymer mixture in contact with different HS matrices as a function of the system fractions η_c, η_p (left panel) and of η_c^r, η_p (right panel) for packing fraction $\eta_m = 0.05$ and size ratios $q = 0.3$, $\sigma_m/\sigma_c = 1$ (corresponding to figure 5). Tielines between coexisting phases have negative slopes in the left panel and are vertical in the right panel.

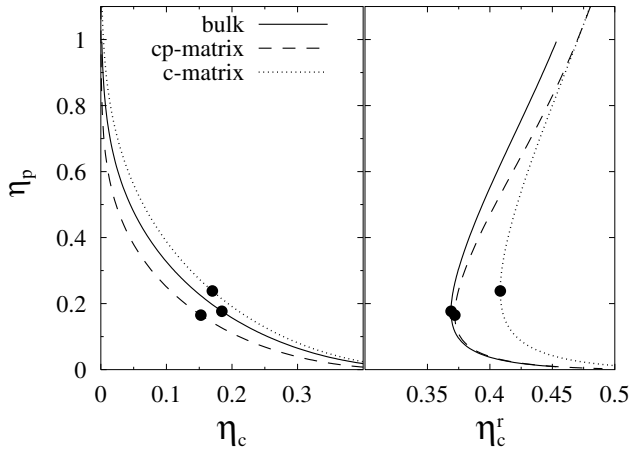

Figure 9. The same as figure 8, but for $q = 0.6$ corresponding to figure 6.

particles. The phase diagram has been calculated on one hand from an FMT-based DF for the full ternary system. On the other hand, we have used an integral-equation approach for the two-component system with effective pair potentials which is obtained by averaging over the polymer degrees of freedom. We have found excellent agreement for the matrix–colloid and the colloid–colloid pair distribution functions obtained via the two theoretical approaches for a system with a rather large matrix packing fraction and not too close to a phase boundary; additional MC results confirm the reliability of the results. We have then calculated the phase diagram for the bulk colloid–polymer mixture and for the situation where this binary mixture is in contact with a matrix that repels colloids and polymers (cp-matrix) or repels solely colloids (c-matrix). We have considered three values of the size ratio q of colloid and polymer particles (0.3, 0.6 and 1). For the two smaller q-values the c-matrix leads—consistently in the ORPA

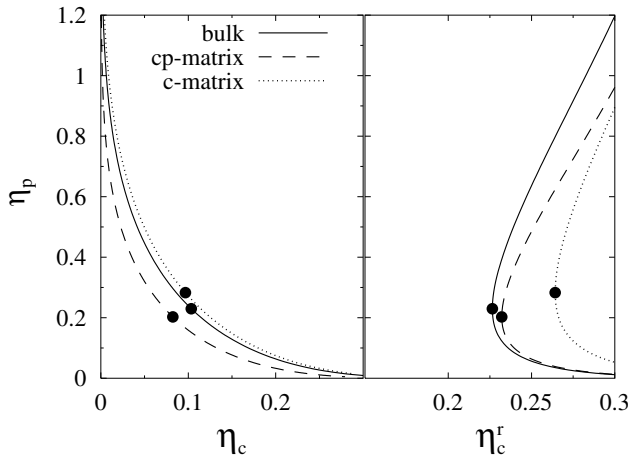

Figure 10. The same as figure 8, but for $q = 1$ corresponding to figure 7.

and DFT—to a considerable shift of the critical point (and consequently of the entire binodal) toward higher polymer packing fractions. For the *cp*-matrix we observe a similar but less pronounced effect. For $q = 1$, inconsistent predictions are observed from the two theories; this can undoubtedly be attributed to a considerable degree to the fact that the mapping of the ternary system onto the binary system with effective pair potentials neglects substantial contributions due to three- and many-body forces. Both approaches predict that the *cp*-matrix and *c*-matrix induce capillary condensation and evaporation, respectively.

Acknowledgments

MS thanks H Löwen for useful discussions and acknowledges support from the DFG within the SFB TR6 'Physics of colloidal dispersions in external fields'. ESP and GK acknowledge financial support by the Österreichische Forschungsfond under project nos P13062-TPH, P15857-TPH and W004.

References

[1] Rosinberg M-L 1999 *New Approaches to Problems in Liquid State Theory (NATO Science Series)* ed C Caccamo, J-P Hansen and G Stell (Dordrecht: Kluwer)
[2] Edwards S F and Anderson P W 1975 *J. Phys. F: Met. Phys.* **5** 965
Edwards S F and Jones C 1976 *J. Phys. A: Math. Gen.* **9** 1595
[3] Given J A 1992 *Phys. Rev.* A **45** 816
[4] Given J A 1992 *J. Chem. Phys.* **96** 2287
[5] Given J A and Stell G 1994 *Physica* A **209** 495
[6] Hansen J-P and McDonald I R 1986 *Theory of Simple Liquids* 2nd edn (New York: Academic)
[7] Rosinberg M-L, Tarjus G and Stell G 1994 *J. Chem. Phys.* **100** 5172
[8] Kierlik E, Rosinberg M-L, Tarjus G and Monson P 1995 *J. Chem. Phys.* **103** 4256
[9] Evans R 1979 *Adv. Phys.* **28** 143
Evans R 1992 *Fundamentals of Inhomogeneous Fluids* ed D Henderson (New York: Dekker) ch 3
[10] Rosenfeld Y 1989 *Phys. Rev. Lett.* **63** 980
[11] Kierlik E and Rosinberg M L 1990 *Phys. Rev.* A **42** 3382
Kierlik E and Rosinberg M L 1991 *Phys. Rev.* A **44** 5025
Phan S, Kierlik E, Rosinberg M L, Bildstein B and Kahl G 1993 *Phys. Rev.* E **48** 618

[12] Rosenfeld Y, Schmidt M, Löwen H and Tarazona P 1996 *J. Phys.: Condens. Matter* **8** L577
Rosenfeld Y, Schmidt M, Löwen H and Tarazona P 1997 *Phys. Rev.* E **55** 4245
[13] Tarazona P and Rosenfeld Y 1997 *Phys. Rev.* E **55** R4873
Tarazona P 2000 *Phys. Rev. Lett.* **84** 694
[14] Schmidt M 1999 *J. Phys.: Condens. Matter* **11** 10 163
[15] Asakura S and Oosawa F 1954 *J. Chem. Phys.* **22** 1255
Vrij A 1976 *Pure Appl. Chem.* **48** 471
[16] Schmidt M, Löwen H, Brader J M and Evans R 2000 *Phys. Rev. Lett.* **85** 1934
Schmidt M, Löwen H, Brader J M and Evans R 2002 *J. Phys.: Condens. Matter* **14** 9353–82
[17] Schmidt M 2001 *Phys. Rev.* E **63** 010101(R)
[18] Cuesta J A 1996 *Phys. Rev. Lett.* **76** 3742
Cuesta J A and Martinez-Raton Y 1997 *Phys. Rev. Lett.* **78** 3681
[19] Rosenfeld Y 1994 *Phys. Rev.* E **50** R3318
Rosenfeld Y 1995 *Mol. Phys.* **86** 637
Schmidt M 2001 *Phys. Rev.* E **63** 050201(R)
von Ferber C and Schmidt M 2001 *Phys. Rev.* E **64** 051115
Brader J M, Esztermann A and Schmidt M 2002 *Phys. Rev.* E **66** 031401
Roth R, van Roij R, Andrienko D, Mecke K R and Dietrich S 2002 *Phys. Rev. Lett.* **89** 088301
[20] Schmidt M 2002 *Phys. Rev.* E at press
[21] Gast A P, Hall C K and Russell W B 1983 *J. Colloid Interface Sci.* **96** 251
[22] Lekkerkerker H N W, Poon W C K, Pusey P N, Stroobants A and Warren P B 1992 *Europhys. Lett.* **20** 559
[23] Dijkstra M, Brader J M and Evans R 1999 *J. Phys.: Condens. Matter* **11** 10 079
[24] Bolhuis P G, Louis A A and Hansen J-P 2002 *Phys. Rev. Lett.* **89** 128302
[25] Brader J M, Dijkstra M and Evans R 2001 *Phys. Rev.* E **63** 041405
Evans R, Brader J M, Roth R, Dijkstra M, Schmidt M and Löwen H 2001 *Phil. Trans. R. Soc.* A **359** 961
Brader J M 2001 *Statistical Mechanics of a Model Colloid–Polymer Mixture* (Bristol: University of Bristol)
Brader J M, Evans R, Schmidt M and Löwen H 2002 *J. Phys.: Condens. Matter* **14** L1
[26] Cuesta J A, Martinez-Raton Y and Tarzona P 2002 *J. Phys.: Condens. Matter* **14** 11965–80
[27] Andersen H C, Chandler D and Weeks J D 1972 *J. Chem. Phys.* **56** 3812
Andersen H C and Chandler D 1972 *J. Chem. Phys.* **57** 1918
[28] Kierlik E, Rosinberg M-L, Tarjus G and Monson P A 1997 *J. Chem. Phys.* **106** 264
[29] Paschinger E, Levesque D, Weis J-J and Kahl G 2001 *Phys. Rev.* E **64** 011502